APPLIED SCIENCES AND ENGINEERING

Generation of charge current from magnetization oscillation via the inverse of voltage-controlled magnetic anisotropy effect

Ambika Shanker Shukla[1], Akanksha Chouhan[1], Rachit Pandey[1], M. Raghupathi[1], Tatsuya Yamamoto[2], Hitoshi Kubota[2], Akio Fukushima[2], Shinji Yuasa[2], Takayuki Nozaki[2], Ashwin A. Tulapurkar[1]*

It is well known that oscillating magnetization induces charge current in a circuit via Faraday's law of electromagnetic induction. New physical phenomena by which magnetization dynamics can produce charge current have gained considerable interest recently. For example, moving magnetization textures, such as domain walls, generates charge current through the spin-motive force. Here, we examine an entirely different effect, which couples magnetization and electric field at the interface between an ultrathin metallic ferromagnet and dielectric. We show that this coupling can convert magnetic energy into electrical energy. This phenomenon is the Onsager reciprocal of the voltage-controlled magnetic anisotropy effect. The effect provides a previously unexplored probe to measure the magnetization dynamics of nanomagnets.

INTRODUCTION

Spintronic technology is based on the control of spins in a magnet. Spin-polarized current has been successfully used to manipulate the magnetization (*1*). Various physical phenomena based on the coupling of spins to phonons (*2*, *3*), orbital angular momentum (*4*–*6*), or heat current (*7*–*9*) have been observed recently, which has led to novel possibilities of switching the magnetization direction. Control of ferromagnetism by electric field is quite attractive (*10*, *11*) as it can lead to ultralow-power writing methods for magnetic memories. Recently, it was found that the magnetic anisotropy of 3d transition ferromagnetic (FM) metals can be controlled by electric field, i.e., by voltage (*12*, *13*). The VCMA (voltage control of magnetic anisotropy) effect has been demonstrated in the technologically important MgO-based magnetic tunnel junctions (*14*, *15*). Voltage-induced FM resonance (FMR) (*16*–*18*) and dynamic switching (*19*–*21*) have shown the potential applications of VCMA for high-speed operations. The electric field–induced modifications of the Curie temperature (*22*), spin-orbit torque (*23*), domain wall, spin-wave propagation (*24*–*27*), interfacial Dzyaloshinskii-Moriya interaction (*28*), and skyrmion motion (*29*, *30*) have also been studied. Designing interfaces to enhance the VCMA effect is an active area of research, such as by an introduction of heavy-metal materials (*31*, *32*) and oxidation control using an ultrathin Mg insertion at CoFeB|MgO interface (*33*).

All the effects in nature have an inverse effect, which can be ascribed to the Onsager reciprocity (*34*). The inverse effects, apart from the interesting physics involved, can also find useful applications (*35*, *36*). Passing a charge current through a wire produces magnetic field. The inverse of this is the electromotive force produced by changing magnetic flux linked with the wire. This concept was generalized to spin motive force, which is responsible for creation of charge current by moving magnetization textures such as domain walls (*37*). Spin pumping is the inverse of the spin transfer torque effect, which results in spin current from oscillating magnetization (*38*). Spin Seebeck effect (*39*) and its inverse spin Peltier effect (*40*) have also been investigated recently. We here show that the Onsager reciprocal of the VCMA effect produces charge current via oscillating magnetization. We measured the scattering matrix (s-matrix) of a two-port device where the transmission of signals between the two ports is based on the VCMA and inverse VCMA effects. By measuring both the effects in the same device, we obtain a direct experimental proof of the reciprocity between these effects.

RESULTS

We fabricated a two-port device as shown schematically in Fig. 1. We deposited stack on Si/SiO_2 substrate: Ta(5)/Ru(5)/Ta(5)/Ru(5)/Ta(9)/CoFeB(1)/CoFe(0.2)/Ir(0.1)/MgO(2.4)/Ta(5)/Ru(7), where the number in parentheses denotes the thickness in nanometers. Note

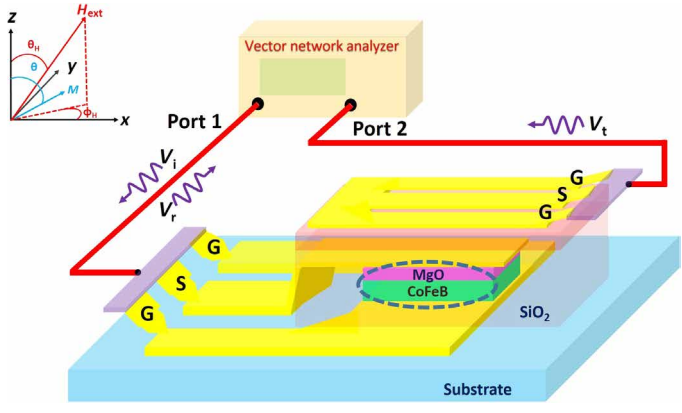

Fig. 1. Schematic of the fabricated two-port device. The top and bottom contacts of the tunnel junction form port 1. Port 2 is a coplanar waveguide electrically insulated from the tunnel junction. The s-matrix of the device is measured as a function of magnetic field applied along polar angle θ_H and azimuthal angle ϕ_H. V_i, V_r, and V_t represent amplitudes of voltage waves incident from port 1, reflected into port 1, and transmitted to port 2, respectively. s_{11} and s_{21} parameters are defined as (V_r/V_i) and (V_t/V_i), respectively.

[1]Solid State Devices Group, Department of Electrical Engineering, Indian Institute of Technology Bombay, Mumbai 400076, India. [2]Spintronics Research Center, National Institute of Advanced Industrial Science and Technology, Tsukuba, Ibaraki 305-8568, Japan.
*Corresponding author. Email: ashwin@ee.iitb.ac.in

that there is only one Ferromagnetic. layer as opposed to two in a magnetic tunnel junction stack. A thin layer of Ir is introduced to enhance the VCMA effect (*41*). We then fabricated tunnel junctions of 3 μm by 80 μm dimension with top and bottom contacts. A coplanar waveguide (CPW) was fabricated on the top, which was electrically insulated from the bottom tunnel junction. The patterning of the device was performed by E-beam lithography and Ar ion milling.

We measured the s-matrix of the device using a vector network analyzer. All the measurements were carried out at room temperature with radio frequency (RF) input power of −20 dBm. The magnetic field was swept along different directions by varying polar angle (θ_H) and azimuthal angle (ϕ_H). The measurement of s_{21} parameter corresponds to the direct VCMA effect. Here, the ac voltage applied to port 1 (tunnel junction port) oscillates magnetization of FM by the VCMA effect. The oscillating magnetization induces ac voltage in the port 2 (CPW) by Faraday's law of electromagnetic induction (*42*). The measurement of s_{12} can be ascribed to the inverse of VCMA effect. Here, the oscillating voltage applied to port 2 creates oscillating current in the CPW, which exerts oscillating magnetic field on the FM. The resultant oscillation of the magnetization of the FM creates voltage in the port 1 by the inverse VCMA effect.

We first present the results of s_{22} measurements, which were carried out to characterize the FMR of the FM film and measure the VCMA coefficient. The absolute value of the s_{22} spectrum measured at a frequency of 3 GHz as a function of magnetic field applied along x axis is shown in Fig. 2A after background subtraction. The peak in the spectrum corresponds to the FMR. The spectrum is well described by the equation $|s_{22}| = A\{\omega_1/\omega_2[(\omega - \omega_0)^2 + (0.5\,\alpha(\omega_1 + \omega_2))^2]\}^{1/2}$, where A is a constant, α is damping parameter,$\omega_1 = \gamma(H_{ext} + H_{//} + H_{\perp})$, $\omega_2 = \gamma(H_{ext} + H_{//})$, and $\omega_0 = \sqrt{\omega_1\omega_2}$. H_{ext} denotes the external magnetic field along the easy axis (x axis here). $H_{//}$ and $H_{\perp}$ denote the anisotropy fields along the easy and hard axis (z axis), respectively. $\gamma = \gamma_0/(1 + \alpha^2)$, where γ_0 denotes the gyromagnetic ratio. The solid black line in Fig. 2A is obtained with $\gamma_0 = 2.2 \times 10^5$ m/A·s, $H_{//} =$ 10 Oe, $H_{\perp} = 400$ Oe, and $\alpha = 0.09$. The inset shows the resonance magnetic field as a function of frequency. The solid line is obtained from the Kittel's formula (*35*), $f_0 = (1/2\pi)\sqrt{\omega_1\omega_2}$, using the same values of parameters. Next, we applied a dc voltage across the tunnel junction and measured the s_{22} spectrum. The absolute value of the s_{22} spectrum at a frequency of 3 GHz (normalized to 0-V data), as a function of magnetic field is shown in Fig. 2B for +0.5 V (cyan), 0 V (magenta), and −0.5 V (green). The shift of the resonance magnetic field is due to the VCMA effect. The applied voltage changes the perpendicular magnetic anisotropy ($H_{\perp}$), which changes the resonance magnetic field as can be seen from the Kittel's equation written above. The VCMA coefficient, which is defined as change in the surface anisotropy energy per unit area per unit electric field, is estimated from the shift to be 100 fJ/V·m. The s_{12} and s_{21} spectra measured at 3-GHz frequency, as a function of external magnetic field swept along $\theta_H = 45°$ and $\phi_H = 0°$ (i.e., magnetic field in the x-z plane) is shown in Fig. 3 (A and B).

The tunnel junction has a resistance due to the tunneling barrier and also capacitance, which includes internal capacitance (i.e., capacitance of top metal layer/MgO/bottom metal layer) and stray capacitance. A model for the tunnel junction is shown in the Supplementary Materials (fig. S3) and is fitted to the reflection coefficient of tunnel junction as a function of frequency to extract the resistance and capacitance. The combination of resistance and capacitance gives rise to a phase shift in the s-parameters, which can be estimated from these parameters. The s-parameter data shown are after background subtraction and correction of the phase. One can see that the imaginary part shows a peak and the real part shows a dispersion curve as a function of magnetic field. The peak and dispersion in the imaginary and real parts of s_{21} signal are due to the FMR excited by VCMA effect and its inductive detection by the CPW. The oscillating voltage across the MgO barrier gives rise to an effective ac magnetic field along z direction. This gives rise to FMR of the FM layer at a certain value of external magnetic field. The oscillating component of magnetization along y direction induces voltage in the top CPW, which is detected as s_{21} signal. On the other hand, the peak and dispersion in the imaginary and real parts of s_{12} signal are due to the FMR excited by Oersted magnetic field created by CPW and its detection via the inverse VCMA effect in the tunnel junction. The oscillating voltage applied to CPW produces ac current, which in turn creates ac magnetic field along y axis on the FM layer. This gives rise to FMR of the FM layer at a certain value of external magnetic field. The component of oscillating magnetization along z axis produces voltage in the tunnel junction via inverse VCMA

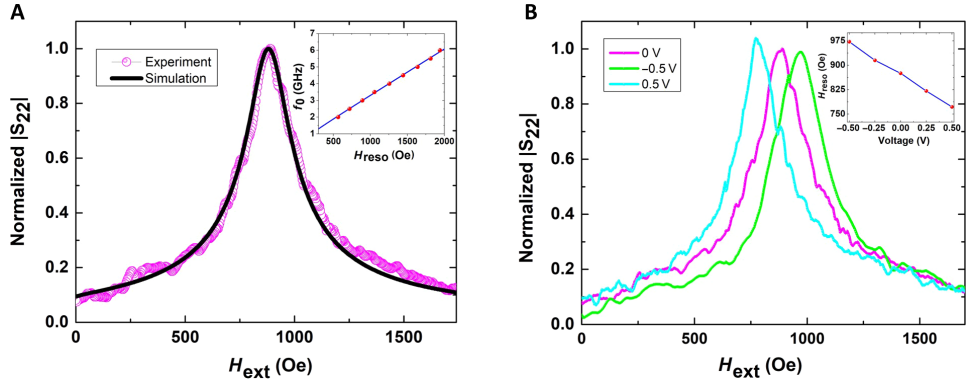

Fig. 2. Measurement of VCMA coefficient by FMR. (**A**) Absolute value of s_{22} parameter at 3 GHz as a function of external dc magnetic field applied along the x axis. The experimental data (magenta circles) are well modeled by the simulation (black curve). The inset shows resonance frequency as a function of a magnetic field. The red points are the experimental data, which are well modeled by the Kittel's equation (blue line). (**B**) Absolute value of s_{22} parameter at 3 GHz as a function of external dc magnetic field applied along the x axis for three values of dc voltages applied across the tunnel junction. The shift of the resonance magnetic field is due to the VCMA effect. The inset shows variation of resonance magnetic field as a function of dc voltage.

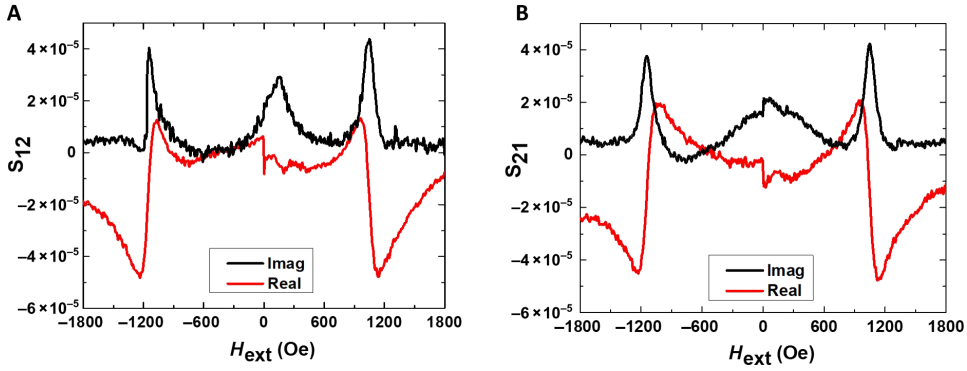

Fig. 3. Real and imaginary parts of the transmission coefficients for magnetic field in *z-x* plane. (**A**) s_{12} and (**B**) s_{21} parameters after background subtraction and phase correction, as a function of external dc magnetic field applied at $\theta_H = 45°$ and $\phi_H = 0°$. The red curve shows the real part, and black curve shows the imaginary part. Both s_{12} and s_{21} parameters are symmetric with respect to magnetic field.

effect, which is detected as s_{12} signal. One can see the following symmetry properties of s_{12} and s_{21}: (i) Both s_{12} and s_{21} are symmetric with respect to the magnetic field, i.e., $s_{12}(H) = s_{12}(-H)$ and $s_{21}(H) = s_{21}(-H)$; and (ii) s_{12} and s_{21} are equal, i.e., $s_{12}(H) = s_{21}(H)$. The absolute value of s_{12} signal as function of θ_H is plotted in Fig. 4. The blue curve shows a fit to the data by $\sin\theta\cos\theta$ dependence, where θ denotes the angle of magnetization with respect to the z axis at resonance magnetic field (note that $\theta \neq \theta_H$.). Such a dependence is expected from the VCMA and inverse VCMA effects and is discussed in section S1.

Figure 5 shows the s_{12} and s_{21} spectra obtained as a function of external magnetic field swept along $\theta_H = 45°$ and $\phi_H = 90°$ (i.e., magnetic field in the *y-z* plane). The symmetry of these spectra with respect to the magnetic field is in stark contrast with respect to the symmetry observed in the spectra for $\phi_H = 0°$ (i.e., magnetic field in the *x-z* plane). One can see the following symmetry properties of s_{12} and s_{21} for $\phi_H = 90°$ case: (i) Both s_{12} and s_{21} are antisymmetric with respect to the magnetic field, i.e., $s_{12}(H) = -s_{12}(-H)$ and $s_{21}(H) = -s_{21}(-H)$; and (ii) s_{12} and s_{21} are equal if magnetic field is reversed, i.e., $s_{12}(H) = s_{21}(-H)$. Thus, in both the cases, $\phi_H = 0°$ and 90°, we can write $s_{12}(H) = s_{21}(-H)$. This is what is expected from the generalized Onsager reciprocity theorem. (The resonance magnetic field for both the cases, $\phi_H = 0°$ and 90°, is larger than $H_\perp$, so that inverting magnetic field also inverts the magnetization direction.) Further, the angular dependence shown in Fig. 4 and antisymmetric nature of s_{12} and s_{21} parameters for $\phi_H = 90°$ case cannot arise from the Oersted magnetic field produced by current in the tunnel junction (also see section S5). These results are well explained by the VCMA and inverse VCMA effects as discussed in section S1.

DISCUSSION

The Onsager reciprocity relations connect the driving forces and the resultant fluxes (*34*). In a two-port circuit, we can consider the currents flowing into them as fluxes that depend linearly on the generalized forces, i.e., voltages applied to the two ports $I_1 = G_{11}V_1 + G_{12}V_2$, $I_2 = G_{21}V_1 + G_{22}V_2$. The Onsager condition $G_{12}(m, H) = G_{21}(-m,-H)$ is equivalent to the condition on s-parameters $s_{12}(m, H) = s_{21}(-m, -H)$. The Onsager relations are valid in the linear response regime. We varied the input power from −20 to −12 dBm and found that the s-parameters are independent of power, indicating that we are operating in the linear regime.

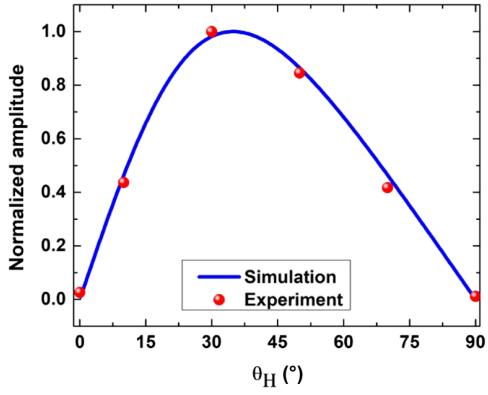

Fig. 4. Angular dependence of s_{21} parameter. Normalized amplitude of s_{21} parameter versus θ_H. The experimental data are well modeled by $\sin\theta\cos\theta$ dependence, where θ denotes the polar angle of magnetization.

The VCMA effect in our devices originates from the modification of electronic structure at the interface between the FM and dielectric. [The high-frequency excitation of magnetization is possible because of the electronic nature of the origin of VCMA (*31*)]. That is, application of electric field modifies the electronic structure and changes the magnetization direction. Conversely, the change in magnetization direction by an external magnetic field should also modify the electronic configuration resulting in electric field. The VCMA effect gives rise to a contribution to the thermodynamic potential per unit volume of FM as $\widetilde{\Phi} = \mu_0 M_s \lambda_{ijk} E_i m_j m_k$ where μ_0 denotes the vacuum permeability, M_s denotes the saturation magnetization, E denotes the electric field at the FM surface, and m denotes the unit vector along the magnetization direction. The third rank tensor λ denotes the coupling between electric field and magnetization. The effective magnetic field on the FM due to this contribution can be written as $H_{\text{eff},k} = -(1/\mu_0 M_s)\frac{\partial \widetilde{\Phi}}{\partial m_k} = -2\lambda_{ijk} E_i m_j$. This shows that electric field changes the anisotropy of the FM. In the present experiment, we have λ_{333} as the only nonzero component, and we take the thermodynamic potential as $\widetilde{\Phi} = \mu_0 M_s \lambda E_z m_z^2$.

Conversely, the same term also gives rise to an effective electric induction (D) given by the derivative of thermodynamic potential per unit volume of dielectric by electric field. As the cross-sectional areas of FM and dielectric are the same, we need to multiply $\widetilde{\Phi}$ by (t_{FM}/t_{MgO}) to get thermodynamic potential per unit volume of dielectric (MgO),

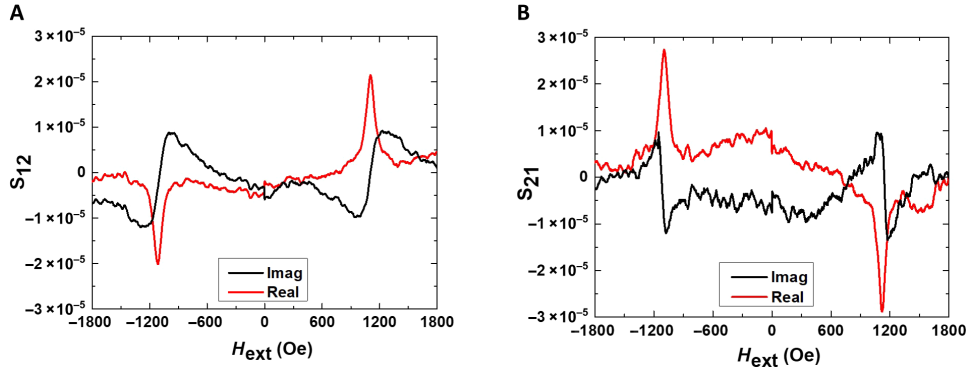

Fig. 5. Real and imaginary parts of the transmission coefficients for magnetic field in *y*-*z* plane. (**A**) s_{12} and (**B**) s_{21} parameters after background subtraction and phase correction, as a function of external dc magnetic field applied at $\theta_H = 45°$ and $\phi_H = 90°$. The red curve shows the real part, and black curve shows the imaginary part. Both s_{12} and s_{21} parameters are antisymmetric with respect to magnetic field.

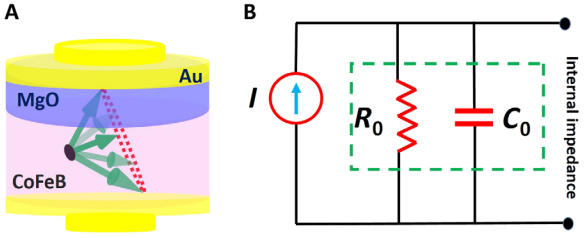

Fig. 6. Model for inverse VCMA effect. (**A**) The magnetization direction of the FM layer is oscillating. (**B**) The oscillating magnetization produces charge current due to the inverse VCMA effect, which can be modeled as a current source *I* with internal impedance of the FM/dielectric tunnel junction in parallel. *I* is given by $\mu_0 M_s(t_{FM}/t_{MgO})\lambda$ area (dm_z^2/dt).

where t denotes the thickness. We get $D_{\text{eff},z} = -\frac{\partial \tilde{\Phi}}{\partial E_z} \frac{t_{FM}}{t_{MgO}} = -\mu_0 M_S \frac{t_{FM}}{t_{MgO}} \lambda m_z^2$. Thus, if z component of magnetization is oscillating, then it gives rise to a current density $J_z = \partial D_{\text{eff},z}/\partial t = -2\mu_0 M_S \frac{t_{FM}}{t_{MgO}} \lambda m_z \frac{dm_z}{dt}$. Thus, the oscillating magnetization gives rise to a current of $I = J_z$ multiplied by the cross-sectional area. This can be represented as a current source I with impedance of the tunnel junction in parallel as shown schematically in Fig. 6.

The inverse VCMA effect can also be derived from the dissipation generated by the VCMA effect or by imposing Onsager reciprocity on the s-matrix. These two methods are discussed in the Supplementary Materials and give the same expression for inverse VCMA effect.

In the present experiment, because of the small MgO thickness, the tunnel junction has low resistance, which is in parallel with the capacitance due to the MgO layer. However, if we increase the MgO thickness, then the tunneling resistance increases exponentially, while the capacitance decreases linearly. Thus, for large MgO thickness, the shunt impedance in Fig. 6 is simply a capacitor (working at a fixed frequency). If the tunnel junction is under open circuit condition, then changing magnetization would simply charge/discharge the capacitor. If the z component of magnetization changes from 0 to ±1, then the amount of charge transfer is $Q = \mu_0 M_S \frac{t_{FM}}{t_{MgO}} \lambda$ area.

Our results demonstrate a novel method for measuring the magnetization dynamics. In the case of tunneling magnetoresistance (TMR)–based detection method, an additional "fixed" FM layer is required, and also we need to pass a dc bias current. Our method does not need any fixed layer and dc bias current. The sensitivity of our method depends on the VCMA coefficient as compared to the TMR ratio in a TMR-based method.

In conclusion, our results provide a new avenue to generate charge current from the magnetization oscillation. This can offer an alternative route to convert magnetic energy into electrical energy and a new probe for the magnetization dynamics of nanomagnets.

MATERIALS AND METHODS

Device fabrication and characterization

Stack of [Ta(5)/Ru(5)/Ta(5)/Ru(5)/Ta(9)/CoFeB(1)/CoFe(0.2)/Ir(0.1)/MgO(2.4)/Ta (5)/Ru(7)] was deposited on Si/SiO_2 substrate (thickness in nanometers). Then, it was patterned into a tunnel junction of 3 μm by 80 μm dimension by following complementary metal-oxide semiconductor–compatible nanofabrication steps using electron beam lithography (EBL), Ar ion milling, and metallization [Cr(5 nm)/Au(150 nm)], followed by Liftoff. For top CPW that is insulated from tunnel junction through RF sputtered 100-nm SiO_2 is patterned by EBL followed by Liftoff. We did deep reactive ion etching (DRIE) for removing back-side silicon under active area (SiO_2 served as a etch stop layer for DRIE). Etched area was then filled with epoxy solution. s-parameters of device were measured using vector network analyzer (VNA) (R&S model no. ZNB-20) at a fixed frequency while sweeping external magnetic field from ±2000 Oe. Measurements were performed for range of frequencies starting from 2 to 6 GHz. Calibration of VNA is performed using CS-8 calibration substrate from GGB Industries. We also used high-frequency GS probes from same company.

SUPPLEMENTARY MATERIALS

Supplementary material for this article is available at http://advances.sciencemag.org/cgi/content/full/6/32/eabc2618/DC1

REFERENCES AND NOTES

1. A. Brataas, A. D. Kent, H. Ohno, Current-induced torques in magnetic materials. *Nat. Mater.* **11**, 372–381 (2012).
2. M. Weiler, L. Dreher, C. Heeg, H. Huebl, R. Gross, M. S. Brandt, S. T. B. Goennenwein, Elastically driven ferromagnetic resonance in nickel thin films. *Phys. Rev. Lett.* **106**, 117601 (2011).
3. S. Mondal, M. A. Abeed, K. Dutta, A. De, S. Sahoo, A. Barman, S. Bandyopadhyay, Hybrid magnetodynamical modes in a single magnetostrictive nanomagnet on a piezoelectric substrate arising from magnetoelastic modulation of precessional dynamics. *ACS Appl. Mater. Interfaces* **10**, 43970–43977 (2018).

4. A. Bose, D. D. Lam, S. Bhuktare, S. Dutta, H. Singh, Y. Jibiki, M. Goto, S. Miwa, A. A. Tulapurkar, Observation of anomalous spin torque generated by a ferromagnet. *Phys. Rev. Appl.* **9**, 064026 (2018).
5. J. Sinova, S. O. Valenzuela, J. Wunderlich, C. H. Back, T. Jungwirth, Spin Hall effects. *Rev. Mod. Phys.* **87**, 1213–1260 (2015).
6. A. Bose, H. Singh, V. K. Kushwaha, S. Bhuktare, S. Dutta, A. A. Tulapurkar, Sign reversal of fieldlike spin-orbit torque in an ultrathin Cr/Ni bilayer. *Phys. Rev. Appl.* **9**, 014022 (2018).
7. A. Bose, A. S. Shukla, S. Dutta, S. Bhuktare, H. Singh, A. A. Tulapurkar, Control of magnetization dynamics by spin-Nernst torque. *Phys. Rev. B.* **98**, 184412 (2018).
8. A. Bose, A. A. Tulapurkar, Recent advances in the spin Nernst effect. *J. Magn. Magn. Mater.* **491**, 165526 (2019).
9. A. Bose, S. Bhuktare, H. Singh, S. Dutta, V. G. Achanta, A. A. Tulapurkar, Direct detection of spin Nernst effect in platinum. *Appl. Phys. Lett.* **112**, 162401 (2018).
10. H. Ohno, D. Chiba, F. Matsukura, T. Omiya, E. Abe, T. Dietl, Y. Ohno, K. Ohtani, Electric-field control of ferromagnetism. *Nature* **408**, 944–946 (2000).
11. D. Chiba, H. Yamanouchi, F. Hatsukura, H. Ohno, Electrical manipulation of magnetization reversal in a ferromagnetic semiconductor. *Science* **301**, 943–945 (2003).
12. M. Weisheit, S. Fähler, A. Marty, Y. Souche, C. Poinsignon, D. Givord, Electric field-induced modification of magnetism in thin-film ferromagnets. *Science* **315**, 349–351 (2007).
13. T. Maruyama, Y. Shiota, T. Nozaki, K. Ohta, N. Toda, M. Mizuguchi, A. A. Tulapurkar, T. Shinjo, M. Shiraishi, S. Mizukami, Y. Ando, Y. Suzuki, Large voltage-induced magnetic anisotropy change in a few atomic layers of iron. *Nat. Nanotechnol.* **4**, 158–161 (2009).
14. T. Nozaki, Y. Shiota, M. Shiraishi, T. Shinjo, Y. Suzuki, Voltage-induced perpendicular magnetic anisotropy change in magnetic tunnel junctions. *Appl. Phys. Lett.* **96**, 022506 (2010).
15. W.-G. Wang, M. Li, S. Hageman, C. L. Chien, Electric-field-assisted switching in magnetic tunneljunctions. *Nat. Mater.* **11**, 64–68 (2012).
16. T. Nozaki, Y. Shiota, S. Miwa, S. Murakami, F. Bonell, S. Ishibashi, H. Kubota, K. Yakushiji, T. Saruya, A. Fukushima, S. Yuasa, T. Shinjo, Y. Suzuki, Electric-field-induced ferromagnetic resonance excitation in an ultrathin ferromagnetic metal layer. *Nat. Phys.* **8**, 491–496 (2012).
17. Y. J. Chen, H. K. Lee, R. Verba, J. A. Katine, I. Barsukov, V. Tiberkevich, J. Q. Xiao, A. N. Slavin, I. N. Krivorotov, Parametric resonance of magnetization excited by electric field. *Nano Lett.* **17**, 572–577 (2017).
18. J. Zhu, J. A. Katine, G. E. Rowlands, Y. J. Chen, Z. Duan, J. G. Alzate, P. Upadhyaya, J. Langer, P. K. Amiri, K. L. Wang, I. N. Krivorotov, Voltage-induced ferromagnetic resonance in magnetic tunnel junctions. *Phys. Rev. Lett.* **108**, 197203 (2012).
19. Y. Shiota, T. Nozaki, F. Bonell, S. Murakami, T. Shinjo, Y. Suzuki, Induction of coherent magnetization switching in a few atomic layers of FeCo using voltage pulses. *Nat. Mater.* **11**, 39–43 (2012).
20. S. Kanai, M. Yamanouchi, S. Ikeda, Y. Nakatani, F. Matsukura, H. Ohno, Electric field-induced magnetization reversal in a perpendicular-anisotropy CoFeB-MgO magnetic tunnel junction. *Appl. Phys. Lett.* **101**, 122403 (2012).
21. T. Yamamoto, T. Nozaki, H. Imamura, Y. Shiota, S. Tamaru, K. Yakushiji, H. Kubota, A. Fukushima, Y. Suzuki, S. Yuasa, Improvement of write error rate in voltage-driven magnetization switching. *J. Phys. D Appl. Phys.* **52**, 164001 (2019).
22. D. Chiba, S. Fukami, K. Shimamura, N. Ishiwata, K. Kobayashi, T. Ono, Electrical control of the ferromagnetic phase transition in cobalt at room temperature. *Nat. Mater.* **10**, 853–856 (2011).
23. Y. Fan, X. Kou, P. Upadhyaya, Q. Shao, L. Pan, M. Lang, X. Che, J. Tang, M. Montazeri, K. Murata, L. Te Chang, M. Akyol, G. Yu, T. Nie, K. L. Wong, J. Liu, Y. Wang, Y. Tserkovnyak, K. L. Wang, Electric-field control of spin-orbit torque in a magnetically doped topological insulator. *Nat. Nanotechnol.* **11**, 352–359 (2016).
24. D. Chiba, M. Kawaguchi, S. Fukami, N. Ishiwata, K. Shimamura, K. Kobayashi, T. Ono, Electric-field control of magnetic domain-wall velocity in ultrathin cobalt with perpendicular magnetization. *Nat. Commun.* **3**, 888 (2012).
25. A. J. Schellekens, A. Van Den Brink, J. H. Franken, H. J. M. Swagten, B. Koopmans, Electric-field control of domain wall motion in perpendicularly magnetized materials. *Nat. Commun.* **3**, 847 (2012).
26. K. Miura, S. Yabuuchi, M. Yamada, M. Ichimura, B. Rana, S. Ogawa, H. Takahashi, Y. Fukuma, Y. Otani, Voltage-induced magnetization dynamics in CoFeB/MgO/CoFeB magnetic tunnel junctions. *Sci. Rep.* **7**, 42511 (2017).
27. B. Rana, Y. Fukuma, K. Miura, H. Takahashi, Y. Otani, Excitation of coherent propagating spin waves in ultrathin CoFeB film by voltage-controlled magnetic anisotropy. *Appl. Phys. Lett.* **111**, 052404 (2017).
28. K. Nawaoka, S. Miwa, Y. Shiota, N. Mizuochi, Y. Suzuki, Voltage induction of interfacial Dzyaloshinskii-Moriya interaction in Au/Fe/MgO artificial multilayer. *Appl. Phys. Express* **8**, 063004 (2015).
29. P. Upadhyaya, G. Yu, P. K. Amiri, K. L. Wang, Electric-field guiding of magnetic skyrmions. *Phys. Rev. B* **92**, 134411 (2015).
30. D. Das, B. Muralidharan, A. Tulapurkar, Skyrmion-based spin-torque nano-oscillator. *J. Magn. Magn. Mater.* **491**, 165608 (2019).
31. T. Nozaki, A. Kozioł-Rachwał, M. Tsujikawa, Y. Shiota, X. Xu, T. Ohkubo, T. Tsukahara, S. Miwa, M. Suzuki, S. Tamaru, H. Kubota, A. Fukushima, K. Hono, M. Shirai, Y. Suzuki, S. Yuasa, Highly efficient voltage control of spin and enhanced interfacial perpendicular magnetic anisotropy in iridium-doped Fe/MgO magnetic tunnel junctions. *NPG Asia Mater.* **9**, e451 (2017).
32. S. Miwa, M. Suzuki, M. Tsujikawa, K. Matsuda, T. Nozaki, K. Tanaka, T. Tsukahara, K. Nawaoka, M. Goto, Y. Kotani, T. Ohkubo, F. Bonell, E. Tamura, K. Hono, T. Nakamura, M. Shirai, S. Yuasa, Y. Suzuki, Voltage controlled interfacial magnetism through platinum orbits. *Nat. Commun.* **8**, 15848 (2017).
33. X. Li, K. Fitzell, D. Wu, C. T. Karaba, A. Buditama, G. Yu, K. L. Wong, N. Altieri, C. Grezes, N. Kioussis, S. Tolbert, Z. Zhang, J. P. Chang, P. Khalili Amiri, K. L. Wang, Enhancement of voltage-controlled magnetic anisotropy through precise control of Mg insertion thickness at CoFeB|MgO interface. *Appl. Phys. Lett.* **110**, 052401 (2017).
34. H. B. G. Casimir, On Onsager's principle of microscopic reversibility. *Rev. Mod. Phys.* **17**, 343–350 (1945).
35. S. Bhuktare, A. S. Shukla, H. Singh, A. Bose, A. A. Tulapurkar, Direct observation of the reciprocity between spin current and phonon interconversion. *Appl. Phys. Lett.* **114**, 052402 (2019).
36. S. Bhuktare, A. Bose, H. Singh, A. A. Tulapurkar, Gyrator based on magneto-elastic coupling at a ferromagnetic/piezoelectric interface. *Sci. Rep.* **7**, 840 (2017).
37. S. E. Barnes, S. Maekawa, Generalization of Faraday's law to include nonconservative spin forces. *Phys. Rev. Lett.* **98**, 246601 (2007).
38. Y. Tserkovnyak, A. Brataas, G. E. W. Bauer, B. I. Halperin, Nonlocal magnetization dynamics in ferromagnetic heterostructures. *Rev. Mod. Phys.* **77**, 1375–1421 (2005).
39. K. Uchida, S. Takahashi, K. Harii, J. Ieda, W. Koshibae, K. Ando, S. Maekawa, E. Saitoh, Observation of the spin Seebeck effect. *Nature* **455**, 778–781 (2008).
40. J. Flipse, F. K. Dejene, D. Wagenaar, G. E. W. Bauer, J. Ben Youssef, B. J. Van Wees, Observation of the spin Peltier effect for magnetic insulators. *Phys. Rev. Lett.* **113**, 027601 (2014).
41. T. Nozaki, T. Yamamoto, S. Tamaru, H. Kubota, A. Fukushima, Y. Suzuki, S. Yuasa, Enhancement in the interfacial perpendicular magnetic anisotropy and the voltage-controlled magnetic anisotropy by heavy metal doping at the Fe/MgO interface. *APL Mater.* **6**, 026101 (2018).
42. T. J. Silva, C. S. Lee, T. M. Crawford, C. T. Rogers, Inductive measurement of ultrafast magnetization dynamics in thin-film Permalloy. *J. Appl. Phys.* **85**, 7849–7862 (1999).

Acknowledgments: We thank Y. Suzuki (Osaka University) for useful discussions. **Funding:** We would like to acknowledge the support of Centre of Excellence in Nanoelectronics (CEN) at Indian Institute of Technology Bombay Nanofabrication facility (IITBNF) and Industrial Research and Consultancy Center (IRCC), IIT Bombay, Mumbai, India for financial support. We acknowledge the support of Department of Science and Technology (DST), Government of India through project no. SR/NM/NS-1112/2016 and Science and Engineering Research Board (SERB) through project no. EMR/2016/007131. **Author contributions:** A.S.S. carried out the microfabrication with help from A.C., R.P., and M.R. The sputtering deposition was optimized by T.Y., H.K., A.F., S.Y., and T.N. T.Y. carried out the deposition of stack. A.S.S. carried out the measurements on the devices. A.S.S. carried out data analysis with help from A.A.T. All authors commented on the manuscript. A.A.T. planned and supervised the project. **Competing interests:** The authors declare that they have no competing interests. **Data and materials availability:** All data needed to evaluate the conclusions in the paper are present in the paper and/or the Supplementary Materials. Additional data related to this paper may be requested from the authors.

Submitted 15 April 2020
Accepted 18 June 2020
Published 5 August 2020
10.1126/sciadv.abc2618

Citation: A. S. Shukla, A. Chouhan, R. Pandey, M. Raghupathi, T. Yamamoto, H. Kubota, A. Fukushima, S. Yuasa, T. Nozaki, A. A. Tulapurkar, Generation of charge current from magnetization oscillation via the inverse of voltage-controlled magnetic anisotropy effect. *Sci. Adv.* **6**, eabc2618 (2020).